ACS APPLIED MATERIALS & INTERFACES

Research Article

www.acsami.org

# Tuning Perovskite Morphology by Polymer Additive for High Efficiency Solar Cell

Chun-Yu Chang,[†] Cheng-Ya Chu,[†] Yu-Ching Huang,[‡] Chien-Wen Huang,[†] Shuang-Yuan Chang,[†] Chien-An Chen,[§] Chi-Yang Chao,[†] and Wei-Fang Su*[,†,§]

[†]Department of Materials Science and Engineering and [§]Institute of Polymer Science and Engineering, National Taiwan University, Taipei 10617, Taiwan

[‡]Institute of Nuclear Energy Research, Taoyuan 32546, Taiwan

Supporting Information

**ABSTRACT:** Solution processable planar heterojunction perovskite solar cell is a very promising new technology for low cost renewable energy. One of the most common cell structures is FTO/$TiO_2$/$CH_3NH_3PbI_{3-x}Cl_x$/spiro-OMeTAD/Au. The main issues of this type of solar cell are the poor coverage and morphology control of the perovskite $CH_3NH_3PbI_{3-x}Cl_x$ film on $TiO_2$. For the first time, we demonstrate that the problems can be easily resolved by using a polymer additive in perovskite precursor solution during the film formation process. A 25% increase in power conversion efficiency at a value of 13.2% is achieved by adding 1 wt % of poly(ethylene glycol) in the perovskite layer using a 150 °C processed $TiO_2$ nanoparticle layer. The morphology of this new perovskite was carefully studied by SEM, XRD, and AFM. The results reveal that the additive controls the size and aggregation of perovskite crystals and helps the formation of smooth film over $TiO_2$ completely. Thus, the $V_{oc}$ and $J_{sc}$ are greatly increased for a high efficiency solar cell. The amount of additive is optimized at 1 wt % due to its insulating characteristics. This research provides a facile way to fabricate a high efficiency perovskite solar cell by the low temperature solution process (<150 °C), which has the advancement of conserving energy over the traditional high temperature sintering $TiO_2$ compact layer device.

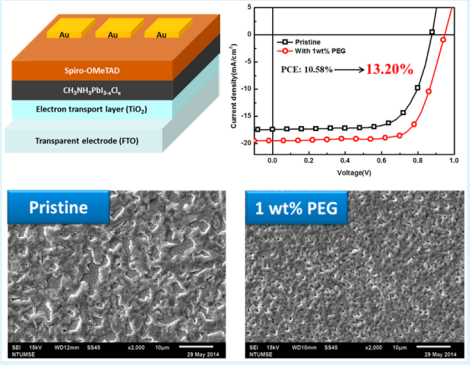


**KEYWORDS:** *perovskite solar cells, polymer additive, morphology, coverage, solution process, $TiO_2$ nanoparticle*

## INTRODUCTION

Organometal trihalide perovskite photovoltaic devices have recently drawn lots of attention due to the properties of high absorption coefficient,[1] broad absorption range,[2] outstanding charge carriers mobility,[3] and long diffusion length.[4] The power conversion efficiency (PCE) of the perovskite solar cells has significantly increased from 3.1% to 20.1% in five years.[5] The organometal trihalide perovskite has the chemical structure of $ABX_3$, where A is the organic cation situated at the eight corner of the unit cell, B is the metal cation located at the body center, and X denotes the halide anion in the six face center.[6] Among these materials, the most extensively investigated ones are $CH_3NH_3PbI_3$ and $CH_3NH_3PbI_{3-x}Cl_x$ because of their long carrier diffusion length of 100 nm and over 1 $\mu$m, respectively.[4] They also exhibit high carrier mobility of about 66 $cm^2/V{\cdot}s$,[3] so the charge carriers can be efficiently transported with low carrier recombination.

Initially, the perovskite solar cells were based on the structure of the solid state dye sensitized solar cell by using perovskite instead of dye as light absorber.[7−11] The mesoporous $TiO_2$ scaffold is used to support the perovskite material. However, this scaffold needs high temperature sintering at about 500 °C, which is a complicated and energy intensive process. Recently, a simple and low cost planar heterojunction structure of perovskite solar cell has been developed without using mesoporous $TiO_2$ scaffold. Two types of cell structure have been investigated: p-i-n planar structure of ITO or FTO/PEDOT:PSS/perovskite material/fullerene derivatives/electron transport layer/Al[12−16] and n-i-p planar structure of FTO/$TiO_2$ dense layer/perovskite material/hole transport layer/Au or Ag.[17,18] The p-i-n planar cell can be manufactured by low temperature solution process, but the PCE of the p-i-n planar cell is relatively lower than that of the n-i-p planar cell.[19] On the other hand, the $TiO_2$ dense layer of the n-i-p planar cell usually requires a high sintering temperature of 500 °C. Recently, the process temperature of the $TiO_2$ dense layer is lowered to <200 °C.[5,20,21]

The main issues of the planar heterojunction perovskite solar cell are the poor coverage and morphology control of the perovskite film via the solution process.[14,15] A.K.Y. Jen et al. utilized 1,8-diiodooctance (DIO) as an additive in the $CH_3NH_3PbI_{3-x}Cl_x$ thin film with the p-i-n planar structure to

Received: January 4, 2015
Accepted: February 13, 2015
Published: February 13, 2015





DOI: 10.1021/acsami.5b00052
ACS Appl. Mater. Interfaces 2015, 7, 4955−4961

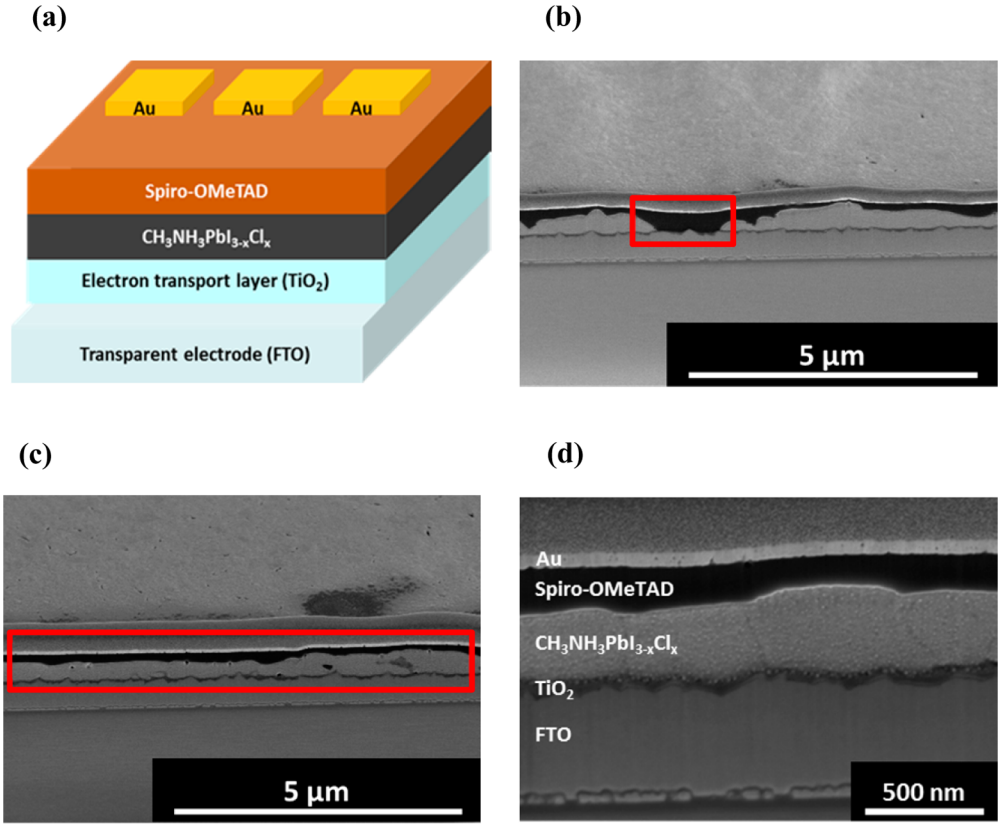


**Figure 1.** (a) Device architecture and (b) SEM cross-sectional image of pristine planar heterojunction perovskite solar cell. (c) SEM cross-sectional image of planar heterojunction perovskite solar cell processed with 1 wt % PEG and (d) the close-up of the image of the red frame in (c).

facilitate homogeneous nucleation and improve the coverage of perovskite film. They showed that the PCE of the cell can be increased from 9.0% to 11.8%.[22] Also, J.Y. Kim et al. reported that they can control the morphology of the perovskite film and obtain uniform crystal domains and smooth surface by using the cosolvent system of γ-butyrolactone (GBL) and *N,N*-dimethylformamide (DMF) in the p-i-n planar cell.[23] The PCE of the device can achieve 8.84% under the optimized mixing ratio. Besides, H.J. Snaith et al. maximized the coverage of perovskite film over the $TiO_2$ dense layer and obtained a high PCE of 11.4% by optimizing the annealing temperature and thickness of perovskite in the n-i-p planar cell.[24]

In this report, we show a simple and novel strategy to significantly increase the PCE of perovskite solar cell using polymer additive. The additive is incorporated into perovskite precursor solution to tune the morphology of the perovskite layer during the film formation process. The poly(ethylene glycol) (PEG) can help the perovskite precursor spread out smoothly. More importantly, the PEG additive can retard the growth and aggregation of perovskite crystals and can reduce the voids between perovskite domains during the phase transformation at 100 °C. That improves the coverage of perovskite film on $TiO_2$ layer. As the results, the current density ($J_{sc}$) of new device is significantly increased from 17.28 to 19.53 mA/cm$^2$. A completed coverage of perovskite film over the $TiO_2$ dense layer is observed that prevents direct contact between $TiO_2$ and hole transport layer. Therefore, the open circuit voltage ($V_{oc}$) of the device is improved from 0.88 to 0.97 V. This is the first report utilizing polymer as an additive to control the morphology of the perovskite layer. The PCE of planar heterojunction perovskite solar cell can achieve more than 25% improvement after optimizing the amount of polymer additive.

## RESULTS AND DISCUSSION

We adopted an n-i-p planar structure to fabricate the perovskite solar cell which is FTO/$TiO_2$ nanoparticle/$CH_3NH_3PbI_{3-x}Cl_x$/2,2′,7,7′-tetrakis(*N,N*-di-*p*-methoxyphenylamine) 9,9′-spirobifluorene (spiro-OMeTAD)/Au, as shown in Figure 1a. The low temperature $TiO_2$ nanoparticle layer was used here according to the literature.[21] It was baked at 150 °C instead of 500 °C used in the conventional $TiO_2$ dense layer which can save energy considerably. The coverage of the perovskite layer is poor for a pristine planar heterojunction perovskite solar cell as shown in the cross-sectional image by scanning electron microscopy (SEM) (Figure 1b). The direct contact of $TiO_2$ nanoparticle with spiro-OMeTAD layer is clearly shown in the red frames marked in Figure 1b. This results in poor device performance. Therefore, we propose to use a polymer additive to improve the coverage of perovskite layer in this study. We selected hydrophilic PEG as an additive which is compatible with perovskite precursor and easily dissolved in DMF. The SEM cross-sectional images of planar heterojunction perovskite solar cell processed with 1 wt % PEG are shown in Figure 1c and d. We can see that the coverage of perovskite film has significantly improved. The systematic investigation has been carried out to optimize the amount of PEG to achieve a high PCE performance of 13.2%. The results are shown and discussed in the following sections.

The current density−voltage curves of the devices are shown in Figure 2, and their performance parameters are summarized in Table 1. The device fabricated with pristine perovskite


DOI: 10.1021/acsami.5b00052
ACS Appl. Mater. Interfaces 2015, 7, 4955−4961

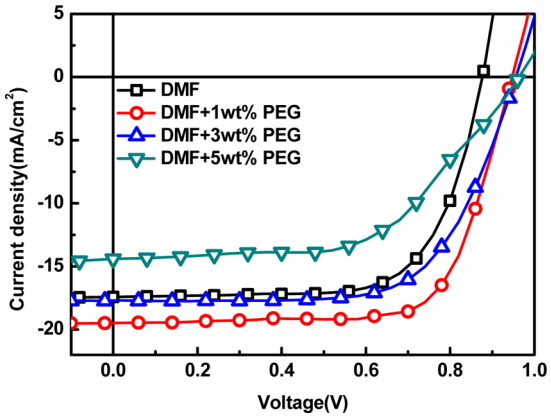


**Figure 2.** Current density−voltage curves of the devices with different amounts of PEG additive in the perovskite film. All the devices were fabricated with a 150 °C processed $TiO_2$ nanoparticle layer.

exhibited $V_{oc}$ of 0.88 V, $J_{sc}$ of 17.28 mA/cm$^2$, fill factor (FF) of 69.28%, and PCE of 10.47%. When the perovskite contained 1 wt % of PEG, the device showed significant improvement in $V_{oc}$ of 0.94 V, $J_{sc}$ of 19.53 mA/cm$^2$, FF of 70.35%, and PCE of 12.90% for an average of 6 devices. The highest PCE among the cells was 13.20%. By further increasing the amount of PEG to 3 wt %, the $V_{oc}$ of the device was improved from 0.94 to 0.97 V; however, the $J_{sc}$ and FF were decreased rapidly and the PCE was only 10.79%. When the perovskite layer contained 5 wt % PEG, the $J_{sc}$ of the device decreased rapidly. It is worth mentioning that measurement of the device with 5 wt % PEG is very difficult and the statistical data showed large standard deviation. We speculate that the difficult measurement and poor reproducibility of the device with 5 wt % PEG is due to the following two reasons. The first reason is the insulating property of PEG. The insulating PEG would hinder the charge transportation in the perovskite layer. Once the amount of PEG additive is overloaded, the charges cannot effectively transport to either $TiO_2$ nanoparticle or spiro-OMeTAD layer and would accumulate or recombine in the perovskite layer. Therefore, the $J_{sc}$ and FF are decreased. Second, because the PEG could fill in the voids and retard the grain growth of the perovskite layer, the high amount of PEG will make the perovskite layer full of individual grains which are separated by the PEG additive. This can be clarified from the SEM images shown in Figure 4c,d. The perovskite layer now cannot maintain the continuous path for charge carrier transport. We conducted more experiments and deduced the explanations for the effects of additive amount on the performance of devices and the coverage of perovskite. These results are summarized in Table 1.

Figure 3a shows the effect of PEG additive on the series resistance ($R_s$) of the devices. For the pristine perovskite film, the $R_s$ is around 5.82 Ω·cm$^2$. The $R_s$ is increased to 7.82 Ω·cm$^2$ with the addition of 1 wt % PEG, and further increased to 13.59 Ω·cm$^2$ and 19.73 Ω·cm$^2$ for 3 and 5 wt % PEG additive, respectively. The results are due to the insulating characteristics of PEG. Figure 3b shows the effect of additive on the performance of $J_{sc}$. It is not in agreement with the increasing trend of $R_s$, which has the maximum $J_{sc}$ with 1 wt % of PEG additive. The changes of morphology of the perovskite film may play a major role on $J_{sc}$. Therefore, the effects of PEG amount in the perovskite layer on the morphology of perovskite film and device performance were investigated in detail.

The SEM was employed to observe the changes of surface morphology and coverage of the perovskite layer by varying the amount of PEG. The perovskite films were fabricated from the precursor solutions containing different amounts of PEG additive on $TiO_2$ nanoparticle/FTO substrates by spin coating and followed by thermal annealing in nitrogen at 100 °C for 1 h. For the pristine perovskite film, the crystals grew and aggregated into large domains with poor coverage. Areas without perovskite coverage can be clearly seen as shown Figure 4a marked by red frames and the coverage of perovskite was 86.44%. The result is in agreement with the cross sectional image of the film shown in Figure 1b. On the other hand, the film containing 1 wt % of PEG, a continuous film with decreased size of domains and voids is observed. The coverage of the perovskite film was significantly improved to 98.13%. It is interesting to note that, when the PEG content was increased to 3 wt %, both size and amount of crystals and voids were increased, but the coverage of perovskite was decreased to 89.20%. This phenomenon is more obvious for the film with 5 wt % of PEG; the coverage was decreased further to 86.46%. We speculate that the 1 wt % PEG helps the spread of precursor solution on the substrate and retards the growth and aggregation of perovskite crystal to have a continuous film with adequate domain sizes. The residual PEG would fill in the space between the perovskite grains. Figure 5a shows the UV−vis absorption spectra of the perovskite films processed with and without 1 wt % PEG. Apparently, the perovskite film processed with 1 wt % PEG has higher absorbance than the pristine one mainly due to the high coverage of the film. The high coverage and continuous perovskite crystalline film absorbs more sunlight and transports charge very efficiently; therefore, the $J_{sc}$ is increased. However, when the amount of PEG is increased to above 1 wt %, the phase separation occurs during the perovskite crystal growth which causes the formation of many voids. Thus, the continuous perovskite crystalline paths cannot be formed for efficient charge transfer and the $J_{sc}$ is decreased.

Atomic force microscopy (AFM) was employed to further investigate the surface roughness of the perovskite film without and with 1 wt % PEG, as represent in Figure S1. The root-mean-square roughness (RMS) of the pristine film is about 117.07 nm, while the film with 1 wt % PEG is reduced to 73.04 nm. Since the PEG can retard the growth and aggregation of perovskite crystals, it is reasonable to speculate that the surface

**Table 1. Characteristics of Perovskite Solar Cells with Different Amounts of PEG Additive in the Perovskite Film**

| Wt% PEG in perovskite | $V_{oc}$ (V) | $J_{sc}$ (mA/cm$^2$) | FF (%) | PCE (%) | PCE max. (%) | $R_s$ (Ω cm$^2$) | Coverage of perovskite (%) |
|---|---|---|---|---|---|---|---|
| 0 | 0.88 ± 0.01 | 17.28 ± 0.16 | 69.28 ± 0.64 | 10.47 ± 0.09 | 10.58 | 5.82 ± 0.41 | 86.44 |
| 1 | 0.94 ± 0.01 | 19.53 ± 0.16 | 70.35 ± 1.25 | 12.90 ± 0.21 | 13.20 | 7.82 ± 1.13 | 98.13 |
| 3 | 0.97 ± 0.01 | 17.89 ± 0.10 | 62.21 ± 3.79 | 10.79 ± 0.46 | 11.23 | 13.59 ± 4.17 | 89.20 |
| 5 | 0.92 ± 0.03 | 9.37 ± 5.17 | 61.32 ± 5.08 | 5.11 ± 2.64 | 7.77 | 74.69 ± 54.29 | 86.46 |
| 5[a] | 0.96 | 14.41 | 55.97 | 7.77 | 7.77 | 19.73 | 86.46 |

[a]It is very difficult to reproduce the device in this composition so we show the best values here.



DOI: 10.1021/acsami.5b00052
ACS Appl. Mater. Interfaces 2015, 7, 4955−4961

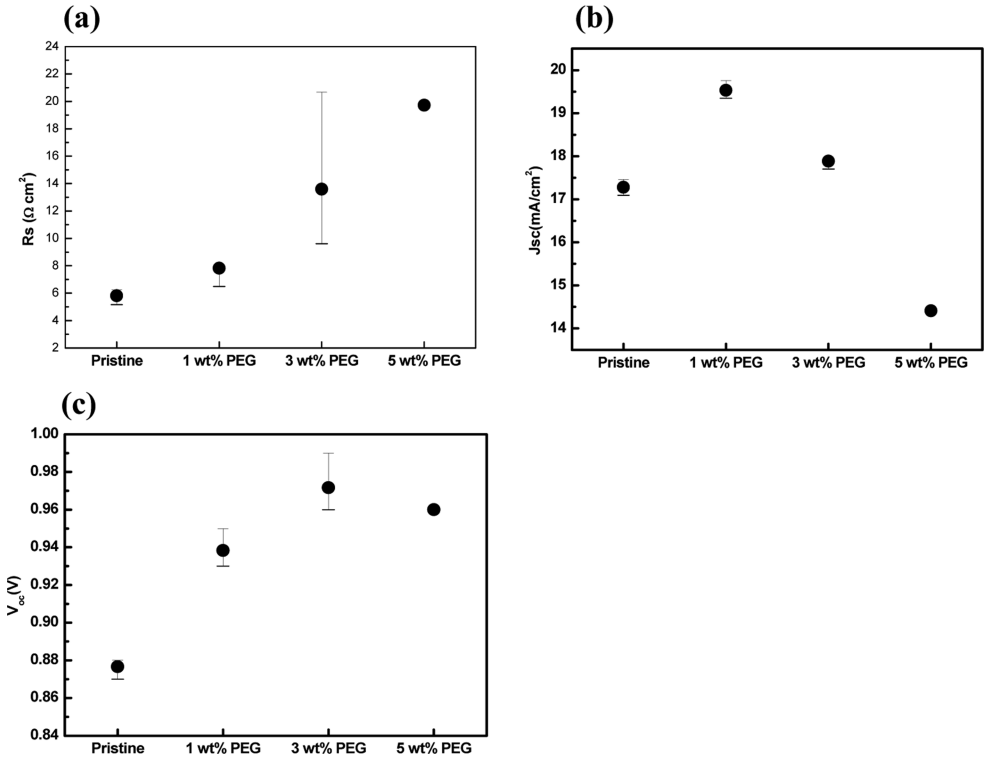


**Figure 3.** Comparison of (a) $R_s$, (b) $J_{sc}$, and (c) $V_{oc}$ for the devices fabricated from perovskite film containing different amount of PEG.

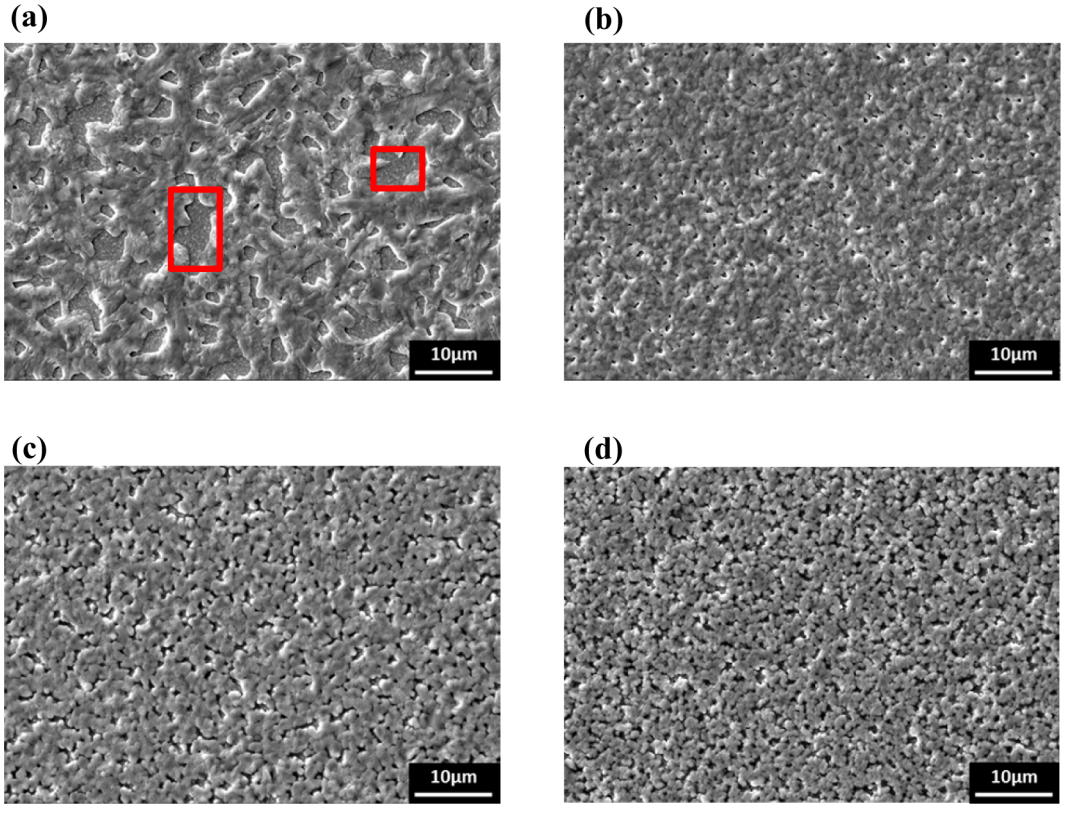


**Figure 4.** SEM images of perovskite films: (a) pristine, (b) with 1 wt %, (c) with 3 wt %, and (d) with 5 wt % of PEG additive on top of the $TiO_2$ nanoparticles layer.

roughness of the film would be reduced with the addition of PEG. The decrease in film roughness has the benefit of improving the interfacial contact between the perovskite film and the spiro-OMeTAD layer for better charge separation and transport.



DOI: 10.1021/acsami.5b00052
ACS Appl. Mater. Interfaces 2015, 7, 4955−4961

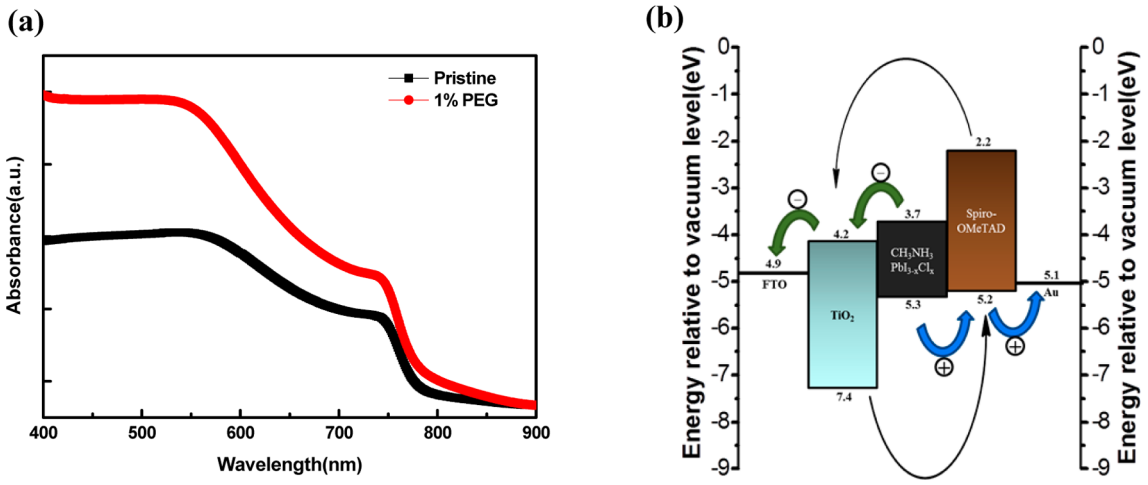


**Figure 5.** (a)UV−vis absorption spectra of perovskite films processed with and without 1 wt % PEG. (b) Energy band diagram of the planar heterojunction perovskite solar cell.

In a short summary, the PEG additive has dual functions to affect the $J_{sc}$ of the devices. The first one is on the positive side from improving the extent of coverage of perovskite film on $TiO_2$ layer. The PEG additive can retard the growth and aggregation of perovskite crystals; thus, a continuous film with good coverage can be obtained. This full coverage perovskite crystalline film can absorb more sunlight and facilitate charge transport. The second one is on the negative side from increasing the $R_s$ of devices with increasing amount of PEG due to its insulating characteristic. As a result, even though the coverage of perovskite film with 3 wt % additive is better than that of the pristine one, its high $R_s$ produces poor $J_{sc}$ performance. Thus, the 1 wt % PEG device reveals the best $J_{sc}$ performance by the compromise between continuous film formation and increasing $R_s$.

Figure 5b shows the energy band diagram of the planar heterojunction perovskite solar cell. Each layer of the device has aligned bandgap; once the sunlight is absorbed by the perovskite layer, excitons are separated at the junction, electrons are transported through the $TiO_2$ nanoparticle layer and out to FTO electrode, and holes are transported through spiro-OMeTAD and out to the Au electrode. The $V_{oc}$ of the device is proportional to the difference between the HOMO of the p-type material ($CH_3NH_3PbI_{3-x}Cl_x$ or spiro-OMeTAD) and LUMO of n-type material ($TiO_2$). If the coverage of the perovskite film in the device is poor, then the $TiO_2$ nanoparticle layer can possibly come into contact with the spiro-OMeTAD layer. Since the HOMO of the spiro-OMeTAD is higher than that of $CH_3NH_3PbI_{3-x}Cl_x$, the direct contact would impart the device with low $V_{oc}$ or even an electrical short. Figure 3c shows the effect of PEG additive on the $V_{oc}$ of the device. The $V_{oc}$ of the device was significantly improved by the addition of PEG, and the $V_{oc}$ was increased with increasing amount of PEG. The improvement in $V_{oc}$ can be easily understood by the good coverage of perovskite from the PEG additive. The high coverage of perovskite can reduce the probability of direct contact of $TiO_2$ and the spiro-OMeTAD layer, which will lead the device with high $V_{oc}$. The increase in $V_{oc}$ with increasing amount of PEG is possible due to the improved coverage achieved with less recombination.

Finally, we also used X-ray diffraction spectrometry (XRD) to examine whether the PEG additive can decrease the bare spots of the $TiO_2$ nanoparticle layer, as represented in Figure 6.

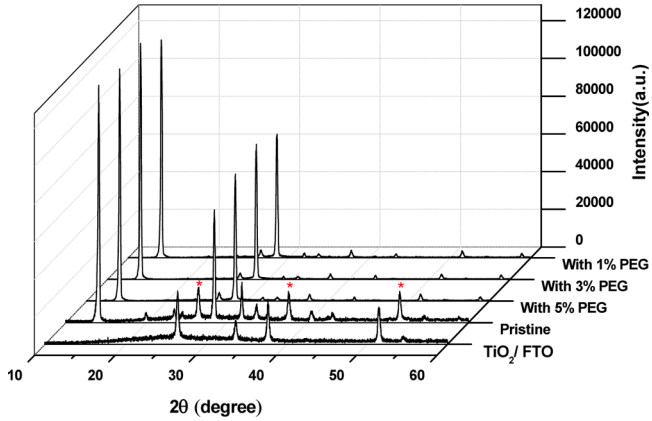


**Figure 6.** XRD patterns of $TiO_2$ nanoparticle/FTO substrate and perovskite films with different amounts of PEG additive on top of the $TiO_2$ nanoparticle layer.

The preparation of the XRD samples was the same as that of the SEM samples. All diffraction results of perovskite films were normalized by the peak at 14.10°, which is the (110) diffraction peak of $CH_3NH_3PbI_{3-x}Cl_x$. The diffraction peaks at 26.46°, 37.71°, and 51.45° are contributed by the $TiO_2$ nanoparticle/FTO substrate. The $CH_3NH_3PbI_{3-x}Cl_x$ films with PEG additive demonstrated a dramatically reduced intensity of $TiO_2$ nanoparticle/FTO substrate peaks as compared to the pristine $CH_3NH_3PbI_{3-x}Cl_x$ film. These results indicate that PEG efficiently improves the coverage of the perovskite layer to avoid the exposure of the $TiO_2$ nanoparticle layer, which is consistent with the SEM results.

## CONCLUSIONS

In conclusion, we have successfully enhanced the PCE of the planar heterojuntion perovskite solar cell from 10.58% to 13.20% by adding 1 wt % of PEG in the perovskite film. All of devices were fabricated at temperature below 150 °C instead of 500 °C commonly used in sintering $TiO_2$ compact layer of the n-i-p planar perovskite solar cell. The PEG additive can tune the morphology of the perovskite layer by retarding the growth and aggregation of perovskite crystals, and promoting the formation of a continuous uniform film. Thus, the absorption of continuous perovskite film is enhanced and $J_{sc}$ is improved.


DOI: 10.1021/acsami.5b00052
ACS Appl. Mater. Interfaces 2015, 7, 4955−4961

However, the $R_s$ of the device is increased by increasing the amount of insulating PEG. The optimal $J_{sc}$ is reached for the device containing 1 wt % of PEG additive. Furthermore, the improvement of the perovskite coverage by the PEG can prevent the direct contact of the $TiO_2$ nanoparticle layer with a spiro-OMeTAD layer that increases the $V_{oc}$. To tune the morphology of perovskite by optimizing the interplay between polymer additive and perovskite, one can improve the performance of the perovskite solar cell dramatically.

## EXPERIMENTAL SECTION

**Materials and Sample Preparation.** The methylammonium iodide (MAI) was synthesized according to the previous report.[8] In brief, 30 mL of hydriodic acid (57 wt % aqueous solution, Acros) was slowly added into the methylamine (33 wt % in ethanol, Acros) with stirring in an ice bath for 2 h in nitrogen. Afterward, the solution was rotary evaporated at 50 °C for 1 h. The resulting precipitate was washed by diethyl ether five times and then recrystallized with ethanol and diethyl ether. Finally, the powder was dried at 60 °C in a vacuum oven for 24 h to obtain pure MAI powder. The $CH_3NH_3PbI_{3-x}Cl_x$ perovskite precursor solution was prepared by mixing as-synthesized MAI powder and lead chloride ($PbCl_2$, 99.999%, Aldrich) at 40 wt % in 1 mL DMF (anhydrous, 99.8%, Sigma-Aldrich) with appropriate amount of PEG (Acros, MW = 6000, 1 wt % to 5 wt % with respect to the content of $CH_3NH_3PbI_{3-x}Cl_x$) and stirring at room temperature. The preparation of spiro-OMeTAD solution was followed by the report of T.K. Kelly et al.[25] First, 104 mg of lithium-bis-(trifluoromethanesulfonyl)imide (Li-TFSI, 99.95%, Aldrich) was dissolved in 0.2 mL acetonitrile (99.5%, Acros) to make a Li-TFSI solution. The spiro-OMeTAD solution can be obtained by dissolving 80 mg spiro-OMeTAD, 28.5 mL 4-*tert*-butylpyridine (96%, Aldrich), and 17.5 mL Li-TFSI solution in 1 mL chlorobenzene (99+%, Acros).

The synthesis of $TiO_2$ nanoparticles was based on the report of H.J. Snaith et al.[21] 2 mL of titanium chloride ($TiCl_4$, 99.9%, Acros) was added slowly into the 8 mL of anhydrous ethanol (99.5%, Shimakyu's Pure. Chemicals) under nitrogen. Afterward, 40 mL of anhydrous benzyl alcohol (99.8%, Sigma-Aldrich) was injected into the $TiCl_4$ solution and reacted at 80 °C for 9 h. The resulting solution was washed by diethyl ether and redispersed in 2-methoxyethanol (99%+, Acros) to form a 10 mg/mL $TiO_2$ nanoparticles solution. 10 mol % of titanium diisopropoxide bis(acetylacetonate) (TiAcAc, 75 wt % in isopropanol, Aldrich) was added into the above $TiO_2$ nanoparticles solution and allowed to stand for 12 h before use.

**Fabrication of the Perovskite Solar Cell.** The planar heterojunction perovskite solar cells were fabricated according to the following procedure. First, the FTO glass (Pilkington, TEC8) was cleaned sequentially with TL-1 ($NH_3$:$H_2O_2$:$H_2O$ = 1:1:5), methanol, and isopropanol and then subjected to plasma treatment for 15 min. The $TiO_2$ nanoparticle solution was spin-coated on the as-cleaned FTO glass by 3000 rpm for 40 s and thermally annealed at 150 °C for 30 min to form the $TiO_2$ layer. Afterward, all the devices were transferred into a nitrogen glovebox. The perovskite precursor solutions with different amounts of PEG additive were then spin-coated over the $TiO_2$ layer with 2000 rpm for 40 s and followed by thermal annealing at 100 °C for 1 h. By using the same concentration (40% by wt) of perovskite precursor solution and the same spin-coating rate of 2000 rpm, the thickness of the perovskite films is ∼400 nm regardless of whether the solution contained PEG or not. Subsequently, the spiro-OMeTAD solution was spin-coated over a perovskite layer at 4000 rpm for 30 s. Finally, gold electrode with thickness of 100 nm was thermally evaporated on top of the device through a shadow mask with 0.09 $cm^2$ active area.

**Characterization.** To measure the photoelectronic performance of the devices, we employed the AM1.5G solar simulator (Newport, 69920) with 100 $mW/cm^{-2}$ input power and recorded the current density−voltage characteristic of the device by the source meter (Keithley 2410). The reported data are measured under the reverse bias (from $V_{oc}$ to $J_{sc}$) with a delay time of 10 ms. For the hysteresis measurement, Figure S2 and Table S1 show the characteristics of perovskite solar cells processed with and without 1 wt % PEG scan in reverse and forward (from $J_{sc}$ to $V_{oc}$) directions. The device showed better performance than the data shown in Figure 2 and Table 1 due to the optimal particle size of the $TiO_2$ nanoparticle by controlling the amount of reactant. The morphology study of the perovskite film was obtained by the SEM (JSM-6510, JEOL) and the coverage of the film was calculated by the program ImageJ. UV−vis absorption spectra were measured by UV−vis spectrophotometer (PerkinElmer Lambda 35). The XRD (Rigaku, TTRAXIII) was used to study the coverage of perovskite film using Cu K$\alpha$ radiation at 50 kV and 300 mA at a scan rate of 10°/min for 2$\theta$ between 10° and 60°. AFM surface height images were taken using Nanoscope III A (Digital Instrument).

## ASSOCIATED CONTENT

### Supporting Information

AFM images of the perovskite layer and scan direction of perovskite solar cell. This material is available free of charge via the Internet at http://pubs.acs.org.

## AUTHOR INFORMATION

### Corresponding Author

*E-mail: suwf@ntu.edu.tw.

### Notes

The authors declare no competing financial interest.

## ACKNOWLEDGMENTS

Financial support obtained from the National Science Council of Taiwan (MOST 103-3113-E-002−011) for this research is highly appreciated.

## REFERENCES

(1) Wolf, S. D.; Holovsky, J.; Moon, S. J.; Löper, P.; Niesen, B.; Ledinsky, M.; Haug, F. J.; Yum, J. H.; Ballif, C. Organometallic Halide Perovskites: Sharp Optical Absorption Edge and Its Relation to Photovoltaic Performance. *J. Phys. Chem. Lett.* **2014**, *5*, 1035−1039.

(2) Eperon, G. E.; Stranks, S. D.; Menelaou, C.; Johnston, M. B.; Herz, L. M.; Snaith, H. J. Formamidinium Lead Trihalide: A Broadly Tunable Perovskite for Efficient Planar Heterojunction Solar Cells. *Energy Environ. Sci.* **2014**, *7*, 982−988.

(3) Kagan, C. R.; Mitzi, D. B.; Dimitrakopoulos, D. Organic-Inorganic Hybrid Materials as Semiconducting Channels in Thin-Film Field-Effect Transistors. *Science* **1999**, *286*, 945−947.

(4) Stranks, S. D.; Eperon, G. E.; Grancini, G.; Menelaou, C.; Alcocer, M. J. P.; Leijtens, T.; Herz, L. M.; Petrozza, A.; Snaith, H. J. Electron-Hole Diffusion Lengths Exceeding 1 Micrometer in an Organometal Trihalide Perovskite Absorber. *Science* **2013**, *342*, 341−344.

(5) NREL, In http://www.nrel.gov/ncpv/.

(6) Gao, P.; Grätzel, M.; Nazeeruddin, M. K. Organohalide Lead Perovskites for Photovoltaic Applications. *Energy Environ. Sci.* **2014**, *7*, 2448−2463.

(7) Kojima, A.; Teshima, K.; Shirai, Y.; Miyasaka, T. Organometal Halide Perovskites as Visible-Light Sensitizers for Photovoltaic Cells. *J. Am. Chem. Soc.* **2009**, *131*, 6050−6051.

(8) Kim, H. S.; Lee, C. R.; Im, J. H.; Lee, K. B.; Moehl, T.; Marchioro, A.; Moon, S. J.; Humphry-Baker, R.; Yum, H. J.; Moser, J. E.; Grätzel, M.; Park, N. G. Lead Iodide Perovskite Sensitized All-Solid-State Submicron Thin Film Mesoscopic Solar Cell with Efficiency Exceeding 9%. *Sci. Rep.* **2012**, *2*, 591−597.

(9) Burschka, J.; Pellet, N.; Moon, S. J.; Humphry-Baker, R.; Gao, P.; Nazeeruddin, M. K.; Grätzel, M. Sequential Deposition As A Route to High-Performance Perovskite-Sensitized Solar Cells. *Nature* **2013**, *499*, 316−319.

(10) Zhu, Z.; Ma, J.; Wang, Z.; Mu, C.; Fan, Z.; Du, L.; Bai, Y.; Fan, L.; Yan, H.; Phillips, D. L.; Yang, S. Efficiency Enhancement of



DOI: 10.1021/acsami.5b00052
*ACS Appl. Mater. Interfaces* 2015, 7, 4955−4961

Perovskite Solar Cells through Fast Electron Extraction: The Role of Graphene Quantum Dots. *J. Am. Chem. Soc.* **2014**, *136*, 3760−3763.
(11) Jeon, N. J.; Lee, J.; Noh, J. H.; Nazeeruddin, M. K.; Grätzel, M.; Seok, S. I. Efficient Inorganic−Organic Hybrid Perovskite Solar Cells Based on Pyrene Arylamine Derivatives as Hole-Transporting Materials. *J. Am. Chem. Soc.* **2013**, *135*, 19087−19090.
(12) Zuo, C.; Ding, L. Bulk heterojunctions push the photoresponse of perovskite solar cells to 970 nm. *J. Mater. Chem. A* **2015**, DOI: 10.1039/C4TA04482G.
(13) You, J.; Hong, Z.; Yang, Y.; Chen, Q.; Cai, M.; Song, T. B.; Chen, C. C.; Lu, S.; Liu, Y.; Zhou, H.; Yang, Y. Low-Temperature Solution-Processed Perovskite Solar Cells with High Efficiency and Flexibility. *ACS Nano* **2014**, *8*, 1674−1680.
(14) Jeng, J. Y.; Chiang, Y. F.; Lee, M. H.; Peng, S. R.; Guo, T. F.; Chen, P.; Wen, T. C. $CH_3NH_3PbI_3$ Perovskite/Fullerene Planar-Heterojunction Hybrid Solar Cells. *Adv. Mater.* **2013**, *25*, 3727−3732.
(15) Docampo, P.; Ball, J. M.; Darwich, M.; Eperon, G. E.; Snaith, H. J. Efficient Organometal Trihalide Perovskite Planar-Heterojunction Solar Cells on Flexible Polymer Substrates. *Nat. Commun.* **2013**, *4*, 2761−2766.
(16) Wang, Q.; Shao, Y.; Dong, Q.; Xiao, Z.; Yuan, Y.; Huang, J. Large Fill-Factor Bilayer Iodine Perovskite Solar Cells Fabricated by A Low-Temperature Solution-Process. *Energy Environ. Sci.* **2014**, *7*, 2359−2365.
(17) Conings, B.; Baeten, L.; Dobbelaere, C. D.; D'Haen, J.; Manca, J.; Boyen, H. G. Perovskite-Based Hybrid Solar Cells Exceeding 10% Efficiency with High Reproducibility Using a Thin Film Sandwich Approach. *Adv. Mater.* **2014**, *26*, 2041−2046.
(18) Liu, M.; Johnston, M. B.; Snaith, H. J. Efficient Planar Heterojunction Perovskite Solar Cells by Vapour Deposition. *Nature* **2013**, *501*, 395−398.
(19) Jeon, N. J.; Lee, H. G.; Kim, Y. C.; Seo, J.; Noh, J. H.; Lee, J.; Seok, S. I. o-Methoxy Substituents in Spiro-OMeTAD for Efficient Inorganic−Organic Hybrid Perovskite Solar Cells. *J. Am. Chem. Soc.* **2014**, *136*, 7837−7840.
(20) Yella, A.; Heiniger, L. P.; Gao, P.; M. Nazeeruddin, K.; Grätzel, M. Nanocrystalline Rutile Electron Extraction Layer Enables Low-Temperature Solution Processed Perovskite Photovoltaics with 13.7% Efficiency. *Nano Lett.* **2014**, *14*, 2591−2596.
(21) Wojciechowski, K.; Saliba, M.; Leijtens, T.; Abate, A.; Snaith, H. J. Sub-150 °C Processed Meso-Superstructured Perovskite Solar Cells with Enhanced Efficiency. *Energy Environ. Sci.* **2014**, *7*, 1142−1147.
(22) Liang, P. W.; Liao, C. Y.; Chueh, C. C.; Zuo, F.; Williams, S. T.; Xin, X. K.; Lin, J.; Jen, A. K. Y. Additive Enhanced Crystallization of Solution-Processed Perovskite for Highly Efficient Planar-Heterojunction Solar Cells. *Adv. Mater.* **2014**, *26*, 3748−3754.
(23) Kim, H. B.; Choi, H.; Jeong, J.; Kim, S.; Walker, B.; Song, S.; Kim, J. Y. Mixed solvents for the optimization of morphology in solution-processed, inverted-type perovskite/fullerene hybrid solar cells. *Nanoscale* **2014**, *6*, 6679−6683.
(24) Eperon, G. E.; Burlakov, V. M.; Docampo, P.; Goriely, A.; Snaith, H. J. Morphological Control for High Performance, Solution-Processed Planar Heterojunction Perovskite Solar Cells. *Adv. Funct. Mater.* **2014**, *24*, 151−157.
(25) Liu, D.; Kelly, T. L. Perovskite Solar Cells with A Planar Heterojunction Structure Prepared Using Room-Temperature Solution Processing Techniques. *Nat. Photonics* **2013**, *8*, 133−138.


DOI: 10.1021/acsami.5b00052
*ACS Appl. Mater. Interfaces* 2015, 7, 4955−4961